Computers and Concrete, *Vol. 21, No. 4 (2018) 431-440*
DOI: https://doi.org/10.12989/cac.2018.21.4.431

Vibration and instability analysis of pipes reinforced by SiO_2 nanoparticles considering agglomeration effects

Hadi Golabchi, Reza Kolahchi* and Mahmood Rabani Bidgoli

Department of Civil Engineering, Islamic Azad University, Jasb Branch, Jasb, Iran

(Received October 30, 2017, Revised December 16, 2017, Accepted December 23, 2017)

Abstract. Fluid velocity analysis on the instability of pipes reinforced by silica nanoparticles (SiO_2) is presented in this paper. Mori-Tanaka model is used for obtaining the effective materials properties of the nanocomposite structure considering agglomeration effects. The well known Navier-Stokes equation is used for obtaining the applied force of fluid to pipe. Based on the Reddy higher-order shear deformation theory, the motion equations are derived based on energy method and Hamilton's principal. The frequency and critical fluid velocity of structure are calculated using differential quadrature method (DQM) so that the effects of different parameters such as volume fractions of SiO2 nanoparticles, SiO2 nanoparticles agglomeration, boundary conditions and geometrical parameters of pipes are considered on the nonlinear vibration and instability of the pipe. Results indicate that increasing the volume fractions of SiO2 nanoparticles, the frequency and critical fluid velocity of the structure are increased. Furthermore, considering SiO2 nanoparticles agglomeration, decreases the frequency and critical fluid velocity of the pipe.

Keywords: vibration and instability; FG-CNTRC pipe; hot fluid; orthotropic visco-elastomeric medium; temperature-dependent

1. Introduction

The pipes conveying fluid can be used in city wastewater. The fluid velocity in the pipe can induced the dynamic load and it is very important for the instability of the structure. However, improving the stiffness of the structure is important for the city wastewater pipes. In this paper, SiO_2 nanoparticles are used for reinforcement of the pipes.

With respect to the developed works in pipes conveying fluid, Paidoussis and Li (1993) studied the dynamic analysis of pipes conveying fluid. Dynamic analysis of anisotropic cylindrical shells containing flowing fluid was studied by Toorani and Lakis (2001). Based on Sanders' non-linear theory, Zhang *et al*. (2002) investigated dynamic analysis of initially tensioned orthotropic thin-walled cylindrical tubes conveying fluid flow. Kadoli and Ganesan (2003) studied vibration and buckling behavior of composite cylindrical shells conveying fluid. The stability of pipe conveying fluid was studied by Wang and Ni (2006). Meng *et al*. (2011) studied the three-dimensional nonlinear dynamics of a fluid-conveying pipe. Dai *et al*. (2012) presented the vibration analysis of three-dimensional (3D) pipelines conveying fluid using transfer matrix method (TMM). Zhang *et al*. (2016) used nonlinear equations of three-dimensional motion for fluid-conveying pipes with general boundary conditions. Based on the Timoshenko beam model, Gu *et al*. (2016) studied dynamic response of a fluid-conveying pipe.

Mechanical analysis of nanostructures has been reported by many researchers (Zemri 2015, Larbi Chaht 2015, Belkorissat 2015, Ahouel 2016, Bounouara 2016, Bouafia 2017, Besseghier 2017, Bellifa 2017, Mouffoki 2017, Khetir 2017). In the field of nanocomposite structures, Vodenitcharova and Zhang (2006) studied bending of a nanocomposite beam using the Airy stress-function method. Large amplitude vibration behavior of nanocomposite cylindrical shells was studied by Shen and Xiang (2012). Rafiee and Moghadam (2012) studied the impact analysis of nanocomposite plates using 3D finite element model. Nonlinear buckling analysis of embedded polymeric temperature-dependent FG-CNTRC microplates resting on an elastic matrix as orthotropic temperature-dependent elastomeric medium was investigated by Kolahchi *et al*. (2015). Thomas and Roy (2015) studied vibration analysis of FG- CNT-reinforced composite shell structures. Mehri *et al*. (2016) studied the bifurcation and vibration responses of a composite truncated conical shell with embedded SWCNTs subjected to an external pressure and axial compression simultaneously. Bayat *et al*. (2016) presented nonlinear analysis of impact response of nanocomposites cylindrical shells reinforced by SWCNTs as FG in thermal environments. Safari Bilouei *et al*. (2016) investigated the nonlinear buckling of straight concrete columns armed with single-walled carbon nanotubes (SWCNTs) resting on foundation. Kolahchi *et al*. (2016) investigated nonlinear dynamic stability analysis of embedded temperature-dependent viscoelastic plates reinforced carbon nanotubes. Motezaker and Kolahchi *et al*. (2017) presented dynamic analysis of a concrete pipes armed with SiO_2 nanoparticles subjected to earthquake load. The structure is modeled with

*Corresponding author, Professor
E-mail: r.kolahchi@gmail.com

ISSN: 1598-8198 (Print), 1598-818X (Online)

Fig. 1 Schematic figure of the pipe reinforced by SiO_2 nanoparticles conveying fluid

first order shear deformation theory (FSDT) of cylindrical shells.

None of the above works have been studied the instability of concrete pipes. In the present study, fluid velocity analysis on the nonlinear instability of pipes reinforced by SiO_2 nanoparticles is presented. The Mori-Tanaka model is used in order to obtain the equivalent material properties of the pipe considering agglomeration effects. Based on the Reddy shell theory, the nonlinear motion equations are obtained based on Hamilton's principal. DQM is applied for obtaining the frequency and critical fluid velocity of the structure. The effects of the volume percent and agglomeration of SiO_2 nanoparticles, boundary conditions and geometrical parameters of the pipes on the frequency and critical fluid velocity of the pipe are shown.

2. Formulation

In Fig. 1, a pipe reinforced by SiO_2 nanoparticles conveying fluid is shown. Agglomeration effects of SiO_2 nanoparticles are considered.

2.1 Reddy theory

There are many new theories for modeling of different structures. Some of the new theories have been used by Tounsi and co-authors (Bessaim 2013, Bouderba 2013, Belabed 2014, Ait Amar Meziane 2014, Zidi 2014, Hamidi 2015, Bourada 2015, Bousahla *et al*. 2016a, b, Beldjelili 2016, Boukhari 2016, Draiche 2016, Bellifa 2015, Attia 2015, Mahi 2015, Ait Yahia 2015, Bennoun 2016, El-Haina 2017, Menasria 2017, Chikh 2017).

Based on Reddy shell theory, the displacement field can be expressed as (Reddy 1984)

$$u_x(x,\theta,z,t)=u\ (x,\theta,t)+z\psi_x(x,\theta,t) -\frac{4z^3}{3h^2}\left(\psi_x(x,\theta,t)+\frac{\partial}{\partial x}w\ (x,\theta,t)\right), \tag{1a}$$

$$u_\theta(x,\theta,z,t)=v(x,\theta,t)+z\psi_\theta(x,\theta,t) -\frac{4z^3}{3h^2}\left(\psi_\theta(x,\theta,t)+\frac{\partial}{R\partial\theta}w\ (x,\theta,t)\right), \tag{1b}$$

$$u_z(x,\theta,z,t)=w(x,\theta,t), \tag{1c}$$

where (u_x, u_θ, u_z) denote the displacement components at an arbitrary point (x,θ,z) in the pipe, and (u,v,w) are the displacement of a material point at (x, θ) on the mid-plane (i.e., z=0) of the pipe along the x-, θ-, and z-directions, respectively; ψ_x and ψ_θ are the rotations of the normal to the mid-plane about θ- and x- directions, respectively. The von Kármán strains associated with the above displacement field can be expressed in the following form

$$\begin{Bmatrix}\varepsilon_{xx}\\ \varepsilon_{\theta\theta}\\ \varepsilon_{x\theta}\\ \varepsilon_{xz}\\ \varepsilon_{\theta z}\end{Bmatrix}=\begin{Bmatrix}\varepsilon^0_{xx}\\ \varepsilon^0_{\theta\theta}\\ \varepsilon^0_{x\theta}\\ \varepsilon^0_{xz}\\ \varepsilon^0_{\theta z}\end{Bmatrix}+z\begin{Bmatrix}\varepsilon^1_{xx}\\ \varepsilon^1_{\theta\theta}\\ \varepsilon^1_{x\theta}\\ \varepsilon^1_{xz}\\ \varepsilon^1_{\theta z}\end{Bmatrix}+z^2\begin{Bmatrix}\varepsilon^2_{xx}\\ \varepsilon^2_{\theta\theta}\\ \varepsilon^2_{x\theta}\\ \varepsilon^2_{xz}\\ \varepsilon^2_{\theta z}\end{Bmatrix}+z^3\begin{Bmatrix}\varepsilon^3_{xx}\\ \varepsilon^3_{\theta\theta}\\ \varepsilon^3_{x\theta}\\ \varepsilon^3_{xz}\\ \varepsilon^3_{\theta z}\end{Bmatrix}, \tag{2}$$

where

$$\begin{Bmatrix}\varepsilon^0_{xx}\\ \varepsilon^0_{\theta\theta}\\ \varepsilon^0_{x\theta}\\ \varepsilon^0_{xz}\\ \varepsilon^0_{\theta z}\end{Bmatrix}=\begin{Bmatrix}\dfrac{\partial u}{\partial x}+\dfrac{1}{2}\left(\dfrac{\partial w}{\partial x}\right)^2\\ \dfrac{\partial v}{R\partial\theta}+\dfrac{w}{R}+\dfrac{1}{2}\left(\dfrac{\partial w}{R\partial\theta}\right)^2\\ \dfrac{\partial v}{\partial x}+\dfrac{\partial u}{R\partial\theta}+\dfrac{\partial w}{\partial x}\dfrac{\partial w}{R\partial\theta}\\ \psi_x+\dfrac{\partial w}{\partial x}\\ \psi_\theta+\dfrac{\partial w}{R\partial\theta}\end{Bmatrix}, \tag{3}$$

$$\begin{Bmatrix}\varepsilon^1_{xx}\\ \varepsilon^1_{\theta\theta}\\ \varepsilon^1_{x\theta}\\ \varepsilon^1_{xz}\\ \varepsilon^1_{\theta z}\end{Bmatrix}=\begin{Bmatrix}\dfrac{\partial\psi_x}{\partial x}\\ \dfrac{\partial\psi_\theta}{R\partial\theta}\\ \dfrac{\partial\psi_x}{R\partial\theta}+\dfrac{\partial\psi_\theta}{\partial x}\\ 0\\ 0\end{Bmatrix}, \tag{4}$$

$$\begin{Bmatrix}\varepsilon^2_{xx}\\ \varepsilon^2_{\theta\theta}\\ \varepsilon^2_{x\theta}\\ \varepsilon^2_{xz}\\ \varepsilon^2_{\theta z}\end{Bmatrix}=\begin{Bmatrix}0\\ 0\\ 0\\ \dfrac{-4}{h^2}\left(\psi_x+\dfrac{\partial w}{\partial x}\right)\\ \dfrac{-4}{h^2}\left(\psi_\theta+\dfrac{\partial w}{R\partial\theta}\right)\end{Bmatrix}, \tag{5}$$

$$\begin{Bmatrix} \varepsilon_{xx}^3 \\ \varepsilon_{\theta\theta}^3 \\ \varepsilon_{x\theta}^3 \\ \varepsilon_{xz}^3 \\ \varepsilon_{\theta z}^3 \end{Bmatrix} = \begin{Bmatrix} \frac{-4}{3h^2}\left(\frac{\partial \psi_x}{\partial x}+\frac{\partial^2 w}{\partial x^2}\right) \\ \frac{-4}{3h^2}\left(\frac{\partial \psi_\theta}{R\partial \theta}+\frac{\partial^2 w}{R^2\partial \theta^2}\right) \\ \frac{-4}{3h^2}\left(\frac{\partial \psi_\theta}{\partial x}+\frac{\partial \psi_x}{R\partial \theta}+2\frac{\partial^2 w}{R\partial x\partial \theta}\right) \\ 0 \\ 0 \end{Bmatrix}, \tag{6}$$

where (ε_{xx}, $\varepsilon_{\theta\theta}$) are the normal strain components and ($\gamma_{\theta z}$, γ_{xz}, $\gamma_{x\theta}$) are the shear strain components.

2.2 Stress-strain relations

The stress-strain relations based on Mori-Tanak model can be written as follows (Mori and Tanaka 1973)

$$\begin{Bmatrix} \sigma_{11} \\ \sigma_{22} \\ \sigma_{33} \\ \sigma_{23} \\ \sigma_{13} \\ \sigma_{12} \end{Bmatrix} = \begin{bmatrix} k+m & l & k-m & 0 & 0 & 0 \\ l & n & l & 0 & 0 & 0 \\ k-m & l & k+m & 0 & 0 & 0 \\ 0 & 0 & 0 & p & 0 & 0 \\ 0 & 0 & 0 & 0 & m & 0 \\ 0 & 0 & 0 & 0 & 0 & p \end{bmatrix} \begin{Bmatrix} \varepsilon_{11} \\ \varepsilon_{22} \\ \varepsilon_{33} \\ \gamma_{23} \\ \gamma_{13} \\ \gamma_{12} \end{Bmatrix} \tag{7}$$

where E_m and υ_m are the Young's modulus and the Poisson's ratio of pipe, respectively. In addition, *k,m,n,l,p*are the stress components, the strain components and the stiffness coefficients. According to the Mori-Tanaka method the stiffness coefficients are given by

$$\begin{aligned} k &= \frac{E_m\{E_m c_m + 2k_r(1+\nu_m)[1+c_r(1-2\nu_m)]\}}{2(1+\nu_m)[E_m(1+c_r-2\nu_m)+2c_m k_r(1-\nu_m-2\nu_m^2)]} \\ l &= \frac{E_m\{c_m\nu_m[E_m+2k_r(1+\nu_m)]+2c_r l_r(1-\nu_m^2)]\}}{(1+\nu_m)[E_m(1+c_r-2\nu_m)+2c_m k_r(1-\nu_m-2\nu_m^2)]} \\ n &= \frac{E_m^2 c_m(1+c_r-c_m\nu_m)+2c_m c_r(k_r n_r - l_r^2)(1+\nu_m)^2(1-2\nu_m)}{(1+\nu_m)[E_m(1+c_r-2\nu_m)+2c_m k_r(1-\nu_m-2\nu_m^2)]} \\ &\quad + \frac{E_m[2c_m^2 k_r(1-\nu_m)+c_r n_r(1+c_r-2\nu_m)-4c_m l_r\nu_m]}{E_m(1+c_r-2\nu_m)+2c_m k_r(1-\nu_m-2\nu_m^2)} \\ p &= \frac{E_m[E_m c_m + 2p_r(1+\nu_m)(1+c_r)]}{2(1+\nu_m)[E_m(1+c_r)+2c_m p_r(1+\nu_m)]} \\ m &= \frac{E_m[E_m c_m + 2m_r(1+\nu_m)(3+c_r-4\nu_m)]}{2(1+\nu_m)\{E_m[c_m+4c_r(1-\nu_m)]+2c_m m_r(3-\nu_m-4\nu_m^2)\}} \end{aligned} \tag{8}$$

where the subscripts *m* and *r* stand for matrix and reinforcement respectively. C_m and C_r are the volume fractions of the matrix and the nanoparticles respectively and k_r, l_r, n_r, p_r, m_r are the Hills elastic modulus for the nanoparticles. Considering agglomeration effects of SiO_2 nanoparticles, the elastic modulus (E) and poison's ratio (υ) can be calculated as (Shi and Feng 2004)

$$E = \frac{9KG}{3K+G}, \tag{9}$$

$$\upsilon = \frac{3K-2G}{6K+2G}. \tag{10}$$

where the effective bulk modulus (K) and effective shear modulus (G) are defiedn in Appendix.

2.3 Energy method

The strain energy can be written as

$$\begin{aligned} U = \frac{1}{2}\int_{\Omega_0}\int_{-h/2}^{h/2}\big(&\sigma_{xx}\varepsilon_{xx}+\sigma_{\theta\theta}\varepsilon_{\theta\theta} \\ &+\sigma_{x\theta}\gamma_{x\theta}+\sigma_{xz}\gamma_{xz}+\sigma_{\theta z}\gamma_{\theta z}\big)dV, \end{aligned} \tag{11}$$

Combining of Eqs. (1)-(10) and (11) yields

$$\begin{aligned} U = \frac{1}{2}\int_{\Omega_0}\Bigg(& N_{xx}\left(\frac{\partial u}{\partial x}+\frac{1}{2}\left(\frac{\partial w}{\partial x}\right)^2\right)+ \\ & N_{\theta\theta}\left(\frac{\partial v}{\partial \theta}+\frac{w}{R}+\frac{1}{2}\left(\frac{\partial w}{R\partial \theta}\right)^2\right)+Q_\theta\left(\frac{\partial w}{R\partial \theta}+\psi_\theta\right) \\ & +Q_x\left(\frac{\partial w}{\partial x}+\psi_x\right)+N_{x\theta}\left(\frac{\partial v}{\partial x}+\frac{\partial u}{R\partial \theta}+\frac{\partial w}{\partial x}\frac{\partial w}{R\partial \theta}\right) \\ & +M_{xx}\frac{\partial \psi_x}{\partial x}+M_{\theta\theta}\frac{\partial \psi_\theta}{R\partial \theta}+M_{x\theta}\left(\frac{\partial \psi_x}{R\partial \theta}+\frac{\partial \psi_\theta}{\partial x}\right) \\ & +K_\theta\left(\frac{-4}{h^2}\left(\psi_\theta+\frac{\partial w}{R\partial \theta}\right)\right)+K_x\left(\frac{-4}{h^2}\left(\psi_x+\frac{\partial w}{\partial x}\right)\right) \\ & +P_{xx}\left(\frac{-4}{3h^2}\left(\frac{\partial \psi_x}{\partial x}+\frac{\partial^2 w}{\partial x^2}\right)\right) \\ & +P_{\theta\theta}\left(\frac{-4}{3h^2}\left(\frac{\partial \psi_\theta}{R\partial \theta}+\frac{\partial^2 w}{R^2\partial \theta^2}\right)\right)+ \\ & P_{x\theta}\left(\frac{\partial \psi_\theta}{\partial x}+\frac{\partial \psi_x}{R\partial \theta}+2\frac{\partial^2 w}{R\partial x\partial \theta}\right)\Bigg)dx d\theta, \end{aligned} \tag{12}$$

where the stress resultant-displacement relations can be written as

$$\begin{Bmatrix} N_{xx} \\ N_{\theta\theta} \\ N_{x\theta} \end{Bmatrix} = \int_{-h/2}^{h/2}\begin{bmatrix} \sigma_{xx} \\ \sigma_{\theta\theta} \\ \sigma_{x\theta} \end{bmatrix} dz, \tag{13}$$

$$\begin{Bmatrix} M_{xx} \\ M_{\theta\theta} \\ M_{x\theta} \end{Bmatrix} = \int_{-h/2}^{h/2}\begin{bmatrix} \sigma_{xx} \\ \sigma_{\theta\theta} \\ \sigma_{x\theta} \end{bmatrix} z dz, \tag{14}$$

$$\begin{Bmatrix} P_{xx} \\ P_{\theta\theta} \\ P_{x\theta} \end{Bmatrix} = \int_{-h/2}^{h/2}\begin{bmatrix} \sigma_{xx} \\ \sigma_{\theta\theta} \\ \sigma_{x\theta} \end{bmatrix} z^3 dz, \tag{15}$$

$$\begin{bmatrix} Q_x \\ Q_\theta \end{bmatrix} = \int_{-h/2}^{h/2}\begin{bmatrix} \sigma_{xz} \\ \sigma_{\theta z} \end{bmatrix} dz, \tag{16}$$

$$\begin{bmatrix} K_x \\ K_\theta \end{bmatrix} = \int_{-h/2}^{h/2}\begin{bmatrix} \sigma_{xz} \\ \sigma_{\theta z} \end{bmatrix} z^2 dz. \tag{17}$$

The kinetic energy of system may be written as

$$K = \frac{\rho}{2}\int_{\Omega_0}\int_{-h/2}^{h/2}\left((\dot{u}_x)^2+(\dot{u}_\theta)^2+(\dot{u}_z)^2\right)dV, \tag{18}$$

The external work due to fluid can be written as

$$W = \int_0^L (P_{Fluid}) w dx, \tag{19}$$

where (Wang and Ni 2009)

$$P_{fluid} = h_f \frac{\partial p_z}{\partial z} = -\rho_f h_f \left(\frac{\partial^2 w}{\partial t^2} + 2v_x \frac{\partial^2 w}{\partial x \partial t} + {v_x}^2 \frac{\partial^2 w}{\partial x^2} \right) + \mu h_f \left(\frac{\partial^3 w}{\partial x^2 \partial t} + \frac{\partial^3 w}{R^2 \partial \theta^2 \partial t} + v_x \left(\frac{\partial^3 w}{\partial x^3} + \frac{\partial^3 w}{R^2 \partial \theta^2 \partial x} \right) \right), \tag{20}$$

where ρ_b and P are fluid mass and flow fluid pressure, respectively; v_x is the mean flow velocity.

The governing equations can be derived by Hamilton's principal as follows

$$\int_0^t (\delta U - \delta W - \delta K) dt = 0. \tag{21}$$

Substituting Eqs. (12)-(19) into Eq. (21) yields the following governing equations

$$\delta u : \frac{\partial N_{xx}}{\partial x} + \frac{\partial N_{x\theta}}{R\partial \theta} = I_0 \frac{\partial^2 u}{\partial t^2} + J_1 \frac{\partial^2 \psi_x}{\partial t^2} - \frac{4I_3}{h^2} \frac{\partial^3 w}{\partial t^2 \partial x}, \tag{22}$$

$$\delta v : \frac{\partial N_{x\theta}}{\partial x} + \frac{\partial N_{\theta\theta}}{R\partial \theta} = I_0 \frac{\partial^2 v}{\partial t^2} + J_1 \frac{\partial^2 \psi_\theta}{\partial t^2} - \frac{4I_3}{h^2} \frac{\partial^3 w}{R\partial t^2 \partial \theta}, \tag{23}$$

$$\begin{aligned} \delta w : & \frac{\partial Q_x}{\partial x} + \frac{\partial Q_\theta}{R\partial \theta} - \frac{4}{h^2}\left(\frac{\partial K_x}{\partial x} + \frac{\partial K_\theta}{R\partial \theta} \right) \\ & + \frac{\partial}{\partial x}\left(N_{xx} \frac{\partial w}{\partial x} + N_{x\theta} \frac{\partial w}{R\partial \theta} \right) \\ & + \frac{\partial}{R\partial \theta}\left(N_{x\theta} \frac{\partial w}{\partial x} + N_{\theta\theta} \frac{\partial w}{R\partial \theta} \right) + \\ & \frac{4}{3h^2}\left(\frac{\partial^2 P_{xx}}{\partial x^2} + 2\frac{\partial^2 P_{x\theta}}{R\partial x \partial \theta} + \frac{\partial^2 P_{\theta\theta}}{R^2 \partial \theta^2} \right) - \frac{N_{\theta\theta}}{R} + q = \\ & I_0 \frac{\partial^2 w}{\partial t^2} - \left(\frac{4}{3h^2} \right)^2 I_6 \left(\frac{\partial^4 w}{\partial x^2 \partial t^2} + \frac{\partial^4 w}{R^2 \partial \theta^2 \partial t^2} \right) + \\ & \frac{4}{3h^2}\left(I_3 \frac{\partial^3 u}{\partial t^2 \partial x} + I_3 \frac{\partial^3 v}{R\partial t^2 \partial \theta} + J_4 \left(\frac{\partial^3 \psi_x}{\partial t^2 \partial x} + \frac{\partial^3 \psi_\theta}{R\partial t^2 \partial \theta} \right) \right), \end{aligned} \tag{24}$$

$$\begin{aligned} \delta \psi_x : & \frac{\partial M_{xx}}{\partial x} + \frac{\partial M_{x\theta}}{R\partial \theta} - \frac{4}{3h^2}\left(\frac{\partial P_{xx}}{\partial x} + \frac{\partial P_{x\theta}}{R\partial \theta} \right) - \\ & Q_x + \frac{4}{h^2} K_x = J_1 \frac{\partial^2 u}{\partial t^2} + K_2 \frac{\partial^2 \psi_x}{\partial t^2} - \frac{4}{3h^2} J_4 \frac{\partial^3 w}{\partial t^2 \partial x}, \end{aligned} \tag{25}$$

$$\begin{aligned} \delta \psi_\theta : & \frac{\partial M_{x\theta}}{\partial x} + \frac{\partial M_{\theta\theta}}{R\partial \theta} - \frac{4}{3h^2}\left(\frac{\partial P_{x\theta}}{\partial x} + \frac{\partial P_{\theta\theta}}{R\partial \theta} \right) - \\ & Q_\theta + \frac{4}{h^2} K_\theta = J_1 \frac{\partial^2 v}{\partial t^2} + K_2 \frac{\partial^2 \psi_\theta}{\partial t^2} - \frac{4}{3h^2} J_4 \frac{\partial^3 w}{R\partial t^2 \partial \theta}, \end{aligned} \tag{26}$$

where

$$I_i = \int_{-h/2}^{h/2} \rho z^i dz \qquad (i = 0,1,...,6), \tag{27}$$

$$J_i = I_i - \frac{4}{3h^2} I_{i+2} \qquad (i = 1,4), \tag{28}$$

$$K_2 = I_2 - \frac{8}{3h^2} I_4 + \left(\frac{4}{3h^2} \right)^2 I_6, \tag{29}$$

Substituting stress relations into Eqs. (13)-(17), the stress resultant-displacement relations can be obtained as follow

$$\begin{aligned} N_{xx} = & A_{11}\left(\frac{\partial u}{\partial x} + \frac{1}{2}\left(\frac{\partial w}{\partial x} \right)^2 \right) + A_{12}\left(\frac{\partial v}{R\partial \theta} + \frac{w}{R} + \frac{1}{2}\left(\frac{\partial w}{R\partial \theta} \right)^2 \right) \\ & + B_{11}\left(\frac{\partial \psi_x}{\partial x} \right) + B_{12}\left(\frac{\partial \psi_\theta}{R\partial \theta} \right) \\ & + E_{11}\left(\frac{-4}{3h^2}\left(\frac{\partial \psi_x}{\partial x} + \frac{\partial^2 w}{\partial x^2} \right) \right) + E_{12}\left(\frac{-4}{3h^2}\left(\frac{\partial \psi_\theta}{R\partial \theta} + \frac{\partial^2 w}{R^2 \partial \theta^2} \right) \right) - N_{xx}^T, \\ N_{\theta\theta} = & A_{12}\left(\frac{\partial u}{\partial x} + \frac{1}{2}\left(\frac{\partial w}{\partial x} \right)^2 \right) + A_{22}\left(\frac{\partial v}{R\partial \theta} + \frac{w}{R} + \frac{1}{2}\left(\frac{\partial w}{R\partial \theta} \right)^2 \right) \\ & + B_{12}\left(\frac{\partial \psi_x}{\partial x} \right) + B_{22}\left(\frac{\partial \psi_\theta}{R\partial \theta} \right) \\ & + E_{12}\left(\frac{-4}{3h^2}\left(\frac{\partial \psi_x}{\partial x} + \frac{\partial^2 w}{\partial x^2} \right) \right) + E_{22}\left(\frac{-4}{3h^2}\left(\frac{\partial \psi_\theta}{R\partial \theta} + \frac{\partial^2 w}{R^2 \partial \theta^2} \right) \right) - N_{\theta\theta}^T, \\ N_{x\theta} = & A_{66}\left(\frac{\partial u}{R\partial \theta} + \frac{\partial v}{\partial x} + \frac{\partial w}{\partial x}\frac{\partial w}{R\partial \theta} \right) + B_{66}\left(\frac{\partial \psi_x}{R\partial \theta} + \frac{\partial \psi_\theta}{\partial x} \right) \\ & + E_{66}\left(\frac{-4}{3h^2}\left(\frac{\partial \psi_\theta}{\partial x} + \frac{\partial \psi_x}{R\partial \theta} + 2\frac{\partial^2 w}{R\partial x \partial \theta} \right) \right), \end{aligned} \tag{30}$$

$$\begin{aligned} M_{xx} = & B_{11}\left(\frac{\partial u}{\partial x} + \frac{1}{2}\left(\frac{\partial w}{\partial x} \right)^2 \right) + B_{12}\left(\frac{\partial v}{R\partial \theta} + \frac{w}{R} + \frac{1}{2}\left(\frac{\partial w}{R\partial \theta} \right)^2 \right) \\ & + D_{11}\left(\frac{\partial \psi_x}{\partial x} \right) + D_{12}\left(\frac{\partial \psi_\theta}{R\partial \theta} \right) \\ & + F_{11}\left(\frac{-4}{3h^2}\left(\frac{\partial \psi_x}{\partial x} + \frac{\partial^2 w}{\partial x^2} \right) \right) + F_{12}\left(\frac{-4}{3h^2}\left(\frac{\partial \psi_\theta}{R\partial \theta} + \frac{\partial^2 w}{R^2 \partial \theta^2} \right) \right) - M_{xx}^T, \\ M_{\theta\theta} = & B_{12}\left(\frac{\partial u}{\partial x} + \frac{1}{2}\left(\frac{\partial w}{\partial x} \right)^2 \right) + B_{22}\left(\frac{\partial v}{R\partial \theta} + \frac{w}{R} + \frac{1}{2}\left(\frac{\partial w}{R\partial \theta} \right)^2 \right) \\ & + D_{12}\left(\frac{\partial \psi_x}{\partial x} \right) + D_{22}\left(\frac{\partial \psi_\theta}{R\partial \theta} \right) \\ & + F_{12}\left(\frac{-4}{3h^2}\left(\frac{\partial \psi_x}{\partial x} + \frac{\partial^2 w}{\partial x^2} \right) \right) + F_{22}\left(\frac{-4}{3h^2}\left(\frac{\partial \psi_\theta}{R\partial \theta} + \frac{\partial^2 w}{R^2 \partial \theta^2} \right) \right) - M_{\theta\theta}^T, \\ M_{x\theta} = & B_{66}\left(\frac{\partial u}{R\partial \theta} + \frac{\partial v}{\partial x} + \frac{\partial w}{\partial x}\frac{\partial w}{R\partial \theta} \right) + D_{66}\left(\frac{\partial \psi_x}{R\partial \theta} + \frac{\partial \psi_\theta}{\partial x} \right) \\ & + F_{66}\left(\frac{-4}{3h^2}\left(\frac{\partial \psi_\theta}{\partial x} + \frac{\partial \psi_x}{R\partial \theta} + 2\frac{\partial^2 w}{R\partial x \partial \theta} \right) \right), \end{aligned} \tag{31}$$

$$\begin{aligned} P_{xx} = & E_{11}\left(\frac{\partial u}{\partial x} + \frac{1}{2}\left(\frac{\partial w}{\partial x} \right)^2 \right) + E_{12}\left(\frac{\partial v}{R\partial \theta} + \frac{w}{R} + \frac{1}{2}\left(\frac{\partial w}{R\partial \theta} \right)^2 \right) \\ & + F_{11}\left(\frac{\partial \psi_x}{\partial x} \right) + F_{12}\left(\frac{\partial \psi_\theta}{R\partial \theta} \right) \\ & + H_{11}\left(\frac{-4}{3h^2}\left(\frac{\partial \psi_x}{\partial x} + \frac{\partial^2 w}{\partial x^2} \right) \right) + H_{12}\left(\frac{-4}{3h^2}\left(\frac{\partial \psi_\theta}{R\partial \theta} + \frac{\partial^2 w}{R^2 \partial \theta^2} \right) \right) - P_{xx}^T, \\ P_{\theta\theta} = & E_{12}\left(\frac{\partial u}{\partial x} + \frac{1}{2}\left(\frac{\partial w}{\partial x} \right)^2 \right) + E_{22}\left(\frac{\partial v}{R\partial \theta} + \frac{w}{R} + \frac{1}{2}\left(\frac{\partial w}{R\partial \theta} \right)^2 \right) \\ & + F_{12}\left(\frac{\partial \psi_x}{\partial x} \right) + F_{22}\left(\frac{\partial \psi_\theta}{R\partial \theta} \right) \end{aligned} \tag{32}$$

$$+H_{12}\left(\frac{-4}{3h^2}\left(\frac{\partial\psi_x}{\partial x}+\frac{\partial^2 w}{\partial x^2}\right)\right)+H_{22}\left(\frac{-4}{3h^2}\left(\frac{\partial\psi_\theta}{R\partial\theta}+\frac{\partial^2 w}{R^2\partial\theta^2}\right)\right)-P^T_{\theta\theta},$$

$$P_{x\theta}=E_{66}\left(\frac{\partial u}{R\partial\theta}+\frac{\partial v}{\partial x}+\frac{\partial w}{\partial x}\frac{\partial w}{R\partial\theta}\right)+F_{66}\left(\frac{\partial\psi_x}{R\partial\theta}+\frac{\partial\psi_\theta}{\partial x}\right)+H_{66}\left(\frac{-4}{3h^2}\left(\frac{\partial\psi_\theta}{\partial x}+\frac{\partial\psi_x}{R\partial\theta}+2\frac{\partial^2 w}{R\partial x\partial\theta}\right)\right),$$

$$Q_x=A_{44}\left(\frac{\partial w}{\partial x}+\psi_x\right)+D_{44}\left(\frac{-4}{h^2}\left(\psi_x+\frac{\partial w}{\partial x}\right)\right),$$

$$Q_\theta=A_{55}\left(\frac{\partial w}{R\partial\theta}+\psi_\theta\right)+D_{55}\left(\frac{-4}{h^2}\left(\psi_\theta+\frac{\partial w}{R\partial\theta}\right)\right), \tag{33}$$

$$K_x=D_{44}\left(\frac{\partial w}{\partial x}+\psi_x\right)+F_{44}\left(\frac{-4}{h^2}\left(\psi_x+\frac{\partial w}{\partial x}\right)\right),$$

$$K_\theta=D_{55}\left(\frac{\partial w}{R\partial\theta}+\psi_\theta\right)+F_{55}\left(\frac{-4}{h^2}\left(\psi_\theta+\frac{\partial w}{R\partial\theta}\right)\right), \tag{34}$$

where

$$A_{ij}=\int_{-h/2}^{h/2}C_{ij}dz,\quad (i,j=1,2,6) \tag{35}$$

$$B_{ij}=\int_{-h/2}^{h/2}C_{ij}zdz, \tag{36}$$

$$D_{ij}=\int_{-h/2}^{h/2}C_{ij}z^2dz, \tag{37}$$

$$E_{ij}=\int_{-h/2}^{h/2}C_{ij}z^3dz, \tag{38}$$

$$F_{ij}=\int_{-h/2}^{h/2}C_{ij}z^4dz, \tag{39}$$

$$H_{ij}=\int_{-h/2}^{h/2}C_{ij}z^6dz, \tag{40}$$

3. DQM

These above governing equations are discetized using DQM, so that they are solved considering the associated boundary conditions to analyze the vibration and instability of the viscose-fluid-conveying nano-composite pipe. The DQM approximates the partial derivative of a function F (representing u, v, w, ψ_x and ψ_θ), with respect to two spatial variables (x and θ) at a given discrete point (x_i, θ_i), as a weighted linear sum of the function values at all discrete points chosen in the solution domain ($0<x<L$, $0<\theta<2\pi$) with $N_x\times N_\theta$ grid points along x and θ axes, respectively. Then, the n[th]-order partial derivative of $F(x,\theta)$ with respect to x, the m[th]-order partial derivative of $F(x,\theta)$ with respect to θ and the $(n+m)$[th]-order partial derivative of $F(x,\theta)$ with respect to both x and θ is expressed discretely at the point (x_i, θ_i) as (Kolahchi *et al*. 2016)

$$\frac{d^n f_x(x_i,\theta_j)}{dx^n}=\sum_{k=1}^{N_x}A_{ik}^{(n)}f(x_k,\theta_j)\qquad n=1,...,N_x-1. \tag{41}$$

$$\frac{d^m f_y(x_i,\theta_j)}{d\theta^m}=\sum_{l=1}^{N_\theta}B_{jl}^{(m)}f(x_i,\theta_l)\quad m=1,...,N_\theta-1. \tag{42}$$

$$\frac{d^{n+m}f_{xy}(x_i,\theta_j)}{dx^n d\theta^m}=\sum_{k=1}^{N_x}\sum_{l=1}^{N_\theta}A_{ik}^{(n)}B_{jl}^{(m)}f(x_k,\theta_l). \tag{43}$$

where $A_{ik}^{(n)}$ and $B_{jl}^{(m)}$ are the weighting coefficients which can be written as

$$A_{ij}^{(1)}=\begin{cases}\dfrac{M(x_i)}{(x_i-x_j)M(x_j)} & for\quad i\neq j,\quad i,j=1,2,...,N_x\\ -\sum\limits_{\substack{j=1\\ i\neq j}}^{N_x}A_{ij}^{(1)} & for\quad i=j,\quad i,j=1,2,...,N_x\end{cases} \tag{44}$$

$$B_{ij}^{(1)}=\begin{cases}\dfrac{P(\theta_i)}{(\theta_i-\theta_j)P(\theta_j)} & for\quad i\neq j,\quad i,j=1,2,...,N_\theta,\\ -\sum\limits_{\substack{j=1\\ i\neq j}}^{N_\theta}B_{ij}^{(1)} & for\quad i=j,\quad i,j=1,2,...,N_\theta\end{cases} \tag{45}$$

In addition, the grid points are

$$X_i=\frac{L}{2}\left[1-\cos\left(\frac{i-1}{N_x-1}\right)\pi\right]\qquad i=1,...,N_x \tag{46}$$

$$\theta_i=\frac{2\pi}{2}\left[1-\cos\left(\frac{i-1}{N_\theta-1}\right)\pi\right]\qquad i=1,...,N_\theta \tag{47}$$

The solution of the motion equations can be assumed as follows

$$d(x,\theta,t)=d_0(x,\theta)e^{\omega t}, \tag{48}$$

where $[d]=[u\ v\ w\ \psi_x\ \psi_y]^T$; ω and t are the frequency and time, respectively. Substituting Eqs. (41)-(43) into the governing equations yeilds

$$\left[[K_L+K_{NL}]+[C]\omega+[M]\omega^2\right][d]=[0], \tag{49}$$

where $[KL]$ and $[K_{NL}]$ are respectively, linear and nonlinear stiffness matrixes; $[C]$ is damp matrix and $[M]$ is the mass matrix. For solving the Eq. (49) and reducing it to the standard form of eigenvalue problem, it is convenient to rewrite Eq. (75) as the following first order variable as

$$\{\dot{Z}\}=[A]\{Z\}, \tag{50}$$

in which the state vector Z and state matrix $[A]$ are defined as

$$Z=\begin{Bmatrix}d_d\\ \dot{d}_d\end{Bmatrix}\ \text{and}\quad [A]=\begin{bmatrix}[0] & [I]\\ -[M^{-1}(K_L+K_{NL})] & -[M^{-1}C]\end{bmatrix}, \tag{51}$$

where [0] and [I] are the zero and unitary matrices, respectively. However, the frequencies obtained from the solution of Eq. (49) are complex due to the damping existed in the presence of the viscous fluid flow. Hence, the results are containing two real and imaginary parts. The real part is corresponding to the system damping, and the imaginary part representing the system natural frequencies.

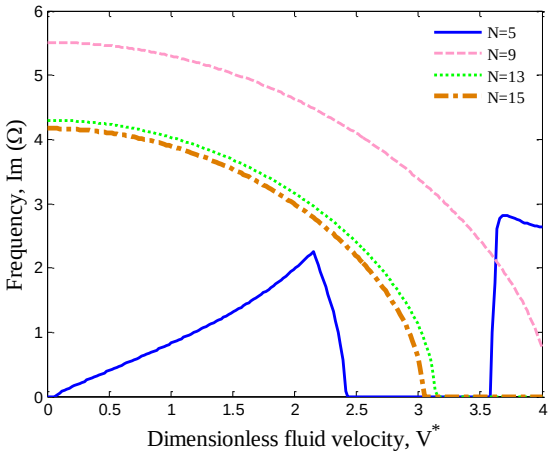

Fig. 2 Convergence of DQM for imaginary part of frequency

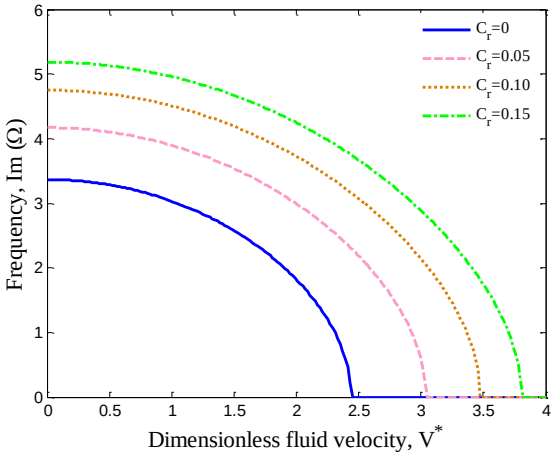

Fig. 4 SiO_2 nanoparticles volume percent effect on the imaginary part of frequency

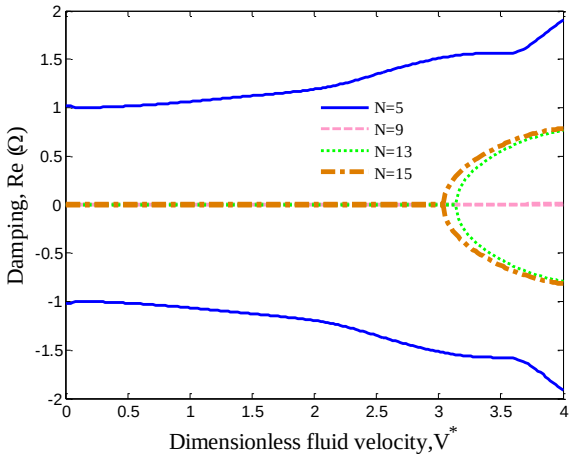

Fig. 3 Convergence of DQM for real part of frequency

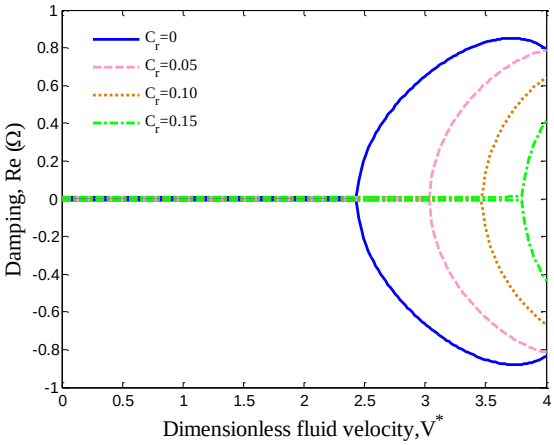

Fig. 5 SiO_2 nanoparticles volume percent effect on the real part of frequency

4. Numerical results and discussion

In this section, the numerical results of nonlinear vibration and instability of nanocomposite pipe conveying fluid are presented. Here, Poly ethylene (PE) is selected for the matrix which have constant Poisson's ratios of v_m=0.3 and Young moduli of E_m=2 GPa. In addition, SiO2 nanoparticles are selected as reinforcements with Poisson's ratios of v_r=0.2 and Young moduli of E_r=66 GPa.

4.1 DQM convergence

The effect of the grid point number in DQM on the imaginary and real parts of dimensionless frequency ($\Omega = \omega L^2 \sqrt{\rho / C_{11}}$) is demonstrated in Figs. 2 and 3 versus the dimensionless fluid velocity ($V = \sqrt{\rho_f / C_{11}}\, v_x$). As can be seen, fast rate of convergence of the method are quite evident and it is found that 15 DQ grid points can yield accurate results.

4.2 The effects of different parameters

Figs. 4 and 5 show the effect of SiO_2 nanoparticles volume percent on the imaginary and real parts of dimensionless eigenvalue. Noted that the imaginary and real parts of dimensionless eigenvalue are dimensionless natural frequency (Im(Ω)) and damping (Re(Ω)), respectively. As can be seen, with increasing the SiO_2 nanoparticles volume percent, the frequency and critical fluid velocity will be increased. It is due to the fact that the stiffness of pipes increases with increasing the SiO_2 nanoparticles volume percent. In addition, Im(Ω) decreases with increasing V, while the Re(Ω) remains zero. These imply that the system is stable. When the natural frequency becomes zero, critical velocity is reached, which the system loses its stability due to the divergence via a pitchfork bifurcation. Hence, the Re(Ω) have the positive real parts, which the system becomes unstable. In this state, both real and imaginary parts of frequency become zero at the same point. Therefore, with increasing flow velocity, system stability decreases and became susceptible to buckling.

The effect of the SiO_2 nanoparticles agglomeration on the dimensionless frequency and damping of the pipe with respect to dimensionless flow velocity is shown in Figs. 6 and 7. It is observed that considering SiO_2 nanoparticles agglomeration, decreases the dimensionless frequency and critical fluid velocity of the pipe. This is due to the fact that considering SiO_2 nanoparticles agglomeration leads to non-

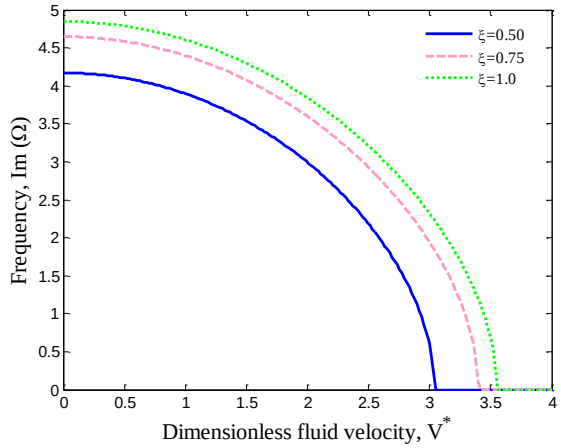

Fig. 6 SiO_2 nanoparticles agglomeration effect on the imaginary part of frequency

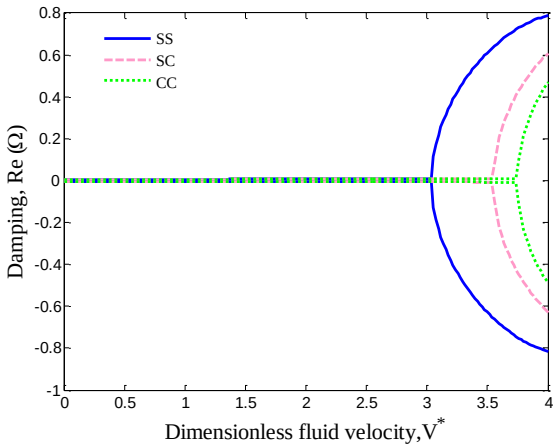

Fig. 9 Boundary condition effect on the real part of frequency

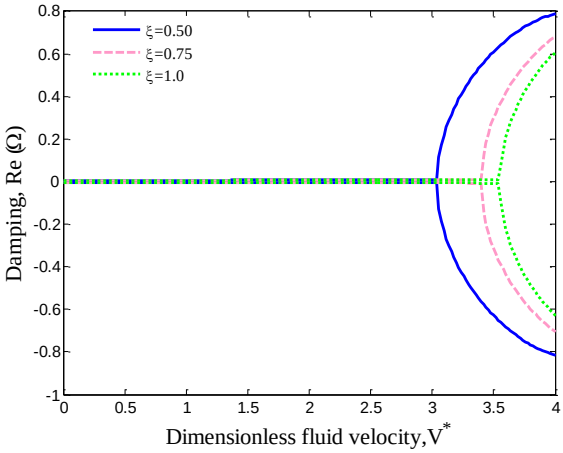

Fig. 7 SiO_2 nanoparticles agglomeration effect on the real part of frequency

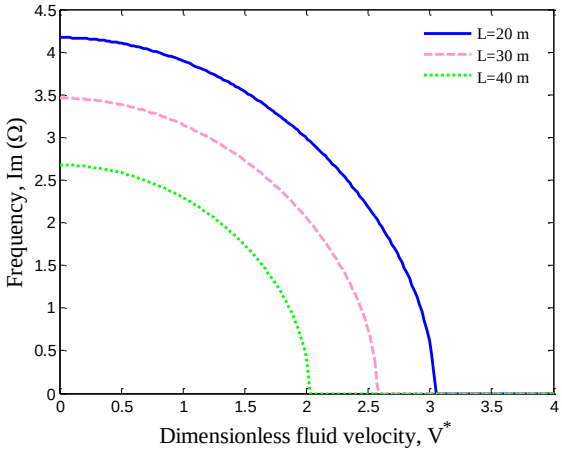

Fig. 10 Pipe length effect on the imaginary part of frequency

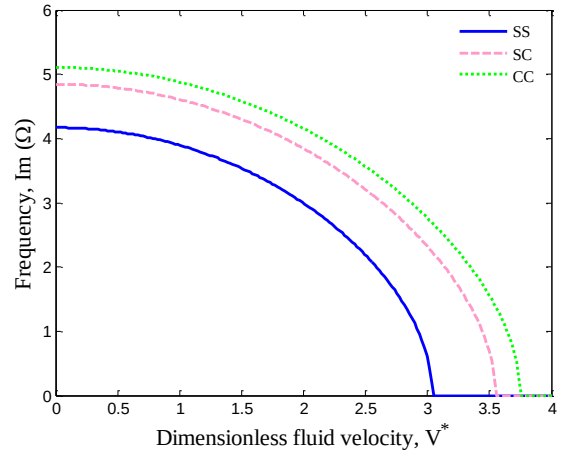

Fig. 8 Boundary condition effect on the imaginary part of frequency

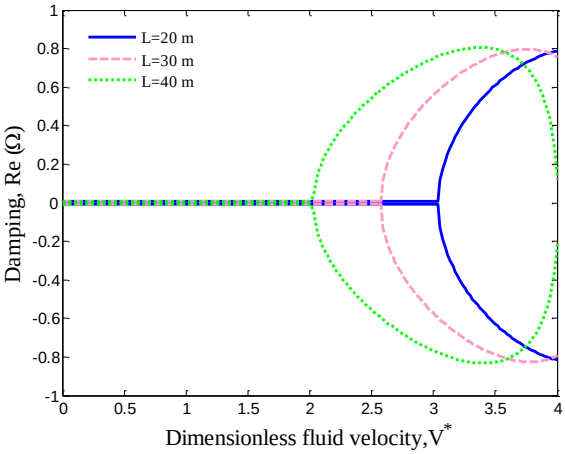

Fig. 11 Pipe length effect on the real part of frequency

homogeneous structure.

The dimensionless frequency and damping of structure versus dimensionless flow velocity are shown in Figs. 8 and 9 for different boundary conditions of CC, SC and SS. It can be seen that the dimensionless frequency and critical fluid velocity of the pipe for CC boundary condition are maximum since the rigidity and stiffness of structure for this type of boundary condition are higher than those of two other cases.

Figs. 10 and 11 indicate the dimensionless frequency and damping of structure versus dimensionless flow velocity for different pipe lengths. It can be seen that with increasing the pipe length, the dimensionless frequency and

damping of the structure are decreased. It is due to the fact that with increasing the pipe length, the stiffness of system decreases.

5. Conclusions

Fluid velocity analysis on the nonlinear vibration and instability of the nanocomposite pipe conveying fluid was presented in this study. The pipe was reinforced by SiO_2 nanoparticles where the effective material properties were determined by Mori-Tanaka model considering agglomeration effects. Based on Reddy shell theory, the motion equations were derived using energy method and Hamilton's principle. DQM was applied for obtaining the frequency and critical fluid velocity of the structure so that the effects of the SiO_2 nanoparticles volume percent and agglomeration, boundary conditions and pipe length were considered. Results indicate that considering SiO_2 nanoparticles agglomeration decreases frequency and critical fluid velocity of the pipe. Furthermore, with increasing SiO_2 nanoparticles volume percent, the frequency and critical fluid velocity of the pipe decrease. In addition, the natural frequency and critical fluid velocity of the pipe decrease with increasing pipe length. In addition, the CC boundary condition lead to higher frequency and critical fluid velocity with respect to other considered boundary conditions.

References

Ahouel, M., Houari, M.S.A., Adda Bedia, E.A. and Tounsi, A. (2016), "Size-dependent mechanical behavior of functionally graded trigonometric shear deformable nanobeams including neutral surface position concept", *Steel Compos. Struct.*, **20**(5), 963-981.

Attia, A., Tounsi, A., Adda Bedia, E.A. and Mahmoud, S.R. (2015), "Free vibration analysis of functionally graded plates with temperature-dependent properties using various four variable refined plate theories", *Steel Compos. Struct.*, **18**(1), 187-212.

Bayat, M.R., Rahmani, O. and Mosavi Mashhadi, M. (2017), "Nonlinear low-velocity impact analysis of functionally graded nanotube-reinforced composite cylindrical shells in thermal environments", *Polym. Compos.*, **39**(3), 730-745.

Belabed, Z., Houari, M.S.A., Tounsi, A., Mahmoud, S.R. and Bég, O.A. (2014), "An efficient and simple higher order shear and normal deformation theory for functionally graded material (FGM) plates", *Compos.: Part B*, **60**, 274-283.

Beldjelili, Y., Tounsi, A. and Mahmoud, S.R. (2016), "Hygro-thermo-mechanical bending of S-FGM plates resting on variable elastic foundations using a four-variable trigonometric plate theory", *Smart Struct. Syst.*, **18**(4), 755-786.

Belkorissat, I., Houari, M.S.A., Tounsi, A. and Hassan, S. (2015), "On vibration properties of functionally graded nano-plate using a new nonlocal refined four variable model", *Steel Compos. Struct.*, **18**(4), 1063-1081.

Bellifa, H., Benrahou, K.H., Bousahla, A.A., Tounsi, A. and Mahmoud, S.R. (2017), "A nonlocal zeroth-order shear deformation theory for nonlinear postbuckling of nanobeams", *Struct. Eng. Mech.*, **62**(6), 695-702.

Bellifa, H., Benrahou, K.H., Hadji, L., Houari, M.S.A. and Tounsi, A. (2016), "Bending and free vibration analysis of functionally graded plates using a simple shear deformation theory and the concept the neutral surface position", *J Braz. Soc. Mech. Sci. Eng.*, **38**(1), 265-275.

Bennoun, M., Houari, M.S.A. and Tounsi, A. (2016), "A novel five variable refined plate theory for vibration analysis of functionally graded sandwich plates", *Mech. Advan. Mater. Struct.*, **23**(4), 423-431.

Bessaim, A., Houari, M.S.A. and Tounsi, A. (2013), "A new higher-order shear and normal deformation theory for the static and free vibration analysis of sandwich plates with functionally graded isotropic face sheets", *J. Sandw. Struct. Mater.*, **15**(6), 671-703.

Besseghier, A., Houari, M.S.A., Tounsi, A. and Hassan, S. (2017), "Free vibration analysis of embedded nanosize FG plates using a new nonlocal trigonometric shear deformation theory", *Smart Struct. Syst.*, **19**(6), 601-614.

Bouafia, Kh., Kaci, A., Houari, M.S.A. and Tounsi, A. (2017), "A nonlocal quasi-3D theory for bending and free flexural vibration behaviors of functionally graded nanobeams", *Smart Struct. Syst.*, **19**, 115-126.

Bouderba, B., Houari, M.S.A. and Tounsi, A. (2013), "Thermomechanical bending response of FGM thick plates resting on Winkler-Pasternak elastic foundations", *Steel Compos. Struct.*, **14**(1), 85-104.

Bouderba, B., Houari, M.S.A., Tounsi, A. and Mahmoud, S.R. (2016b), "Thermal stability of functionally graded sandwich plates using a simple shear deformation theory", *Struct. Eng. Mech.*, **58**(3), 397-422.

Boukhari, A., Atmane, H.A., Tounsi, A., Adda Bedia, E.A. and Mahmoud, S.R. (2016), "An efficient shear deformation theory for wave propagation of functionally graded material plates", *Struct. Eng. Mech.*, **57**(5), 837-859.

Bounouara, F., Benrahou, K.H., Belkorissat, I. and Tounsi, A. (2016), "A nonlocal zeroth-order shear deformation theory for free vibration of functionally graded nanoscale plates resting on elastic foundation", *Steel Compos. Struct.*, **20**(2), 227-249.

Bourada, M., Kaci, A., Houari, M.S.A. and Tounsi, A. (2015), "A new simple shear and normal deformations theory for functionally graded beams", *Steel Compos. Struct.*, **18**(2), 409-423.

Bousahla, A.A., Benyoucef, S., Tounsi, A. and Mahmoud, S.R. (2016a), "On thermal stability of plates with functionally graded coefficient of thermal expansion", *Struct. Eng. Mech.*, **60**(2), 313-335.

Chikh, A., Tounsi, A., Hebali, H. and Mahmoud, S.R. (2017), "Thermal buckling analysis of cross-ply laminated plates using a simplified HSDT", *Smart Struct. Syst.*, **19**(3), 289-297.

Dai, H.L., Wang, L., Qian, Q. and Gan, J. (2012), "Vibration analysis of three-dimensional pipes conveying fluid with consideration of steady combined force by transfer matrix method", *Appl. Math. Comput.*, **219**, 2453-2464.

Draiche, K., Tounsi, A. and Mahmoud, S.R. (2016), "A refined theory with stretching effect for the flexure analysis of laminated composite plates", *Geomech. Eng.*, **11**, 671-690.

El-Haina, F., Bakora, A., Bousahla, A.A. and Hassan, S. (2017), "A simple analytical approach for thermal buckling of thick functionally graded sandwich plates", *Struct. Eng. Mech.*, **63**(5), 585-595.

Gu, J., Tianqi, M. and Menglan, D. (2016), "Effect of aspect ratio on the dynamic response of a fluid-conveying pipe using the Timoshenko beam model", *Ocean Eng.*, **114**, 185-191.

Hamidi, A., Houari, M.S.A., Mahmoud, S.R. and Tounsi, A. (2015), "A sinusoidal plate theory with 5-unknowns and stretching effect for thermomechanical bending of functionally graded sandwich plates", *Steel Compos. Struct.*, **18**(1), 235-253.

Kadoli, R. and Ganesan, N. (2003), "Free vibration and buckling analysis of composite cylindrical shells conveying hot fluid",

Compos. Struct., **60**, 19-32.
Khetir, H., Bouiadjra, M.B., Houari, M.S.A., Tounsi, A. and Mahmoud, S.R. (2017), "A new nonlocal trigonometric shear deformation theory for thermal buckling analysis of embedded nanosize FG plates", *Struct. Eng. Mech.*, **64**(4), 391-402.
Kolahchi, R., Rabani Bidgoli, M., Beygipoor, Gh. and Fakhar, M.H. (2015), "A nonlocal nonlinear analysis for buckling in embedded FG-SWCNT-reinforced microplates subjected to magnetic field", *J. Mech. Sci. Technol.*, **29**, 3669-3677.
Kolahchi, R., Safari, M. and Esmailpour, M. (2016), "Dynamic stability analysis of temperature-dependent functionally graded CNT-reinforced visco-plates resting on orthotropic elastomeric medium", *Compos. Struct.*, **150**, 255-265.
Larbi Chaht, F., Kaci, A., Houari, M.S.A. and Hassan, S. (2015), "Bending and buckling analyses of functionally graded material (FGM) size-dependent nanoscale beams including the thickness stretching effect", *Steel Compos. Struct.*, **18**(2), 425 -442.
Mahi, A., Bedia, E.A.A. and Tounsi, A. (2015), "A new hyperbolic shear deformation theory for bending and free vibration analysis of isotropic, functionally graded, sandwich and laminated composite plates", *Appl. Math. Model.*, **39**, 2489-2508.
Mehri, M., Asadi, H. and Wang, Q. (2016), "Buckling and vibration analysis of a pressurized CNT reinforced functionally graded truncated conical shell under an axial compression using HDQ method", *Comput. Meth. Appl. Mech. Eng.*, **303**, 75-100.
Menasria, A., Bouhadra, A., Tounsi, A. and Hassan, S. (2017), "A new and simple HSDT for thermal stability analysis of FG sandwich plates", *Steel Compos. Struct.*, **25**(2), 157-175.
Meng, D., Guo, H. and Xu, S. (2011), "Non-linear dynamic model of a fluid-conveying pipe undergoing overall motions", *Appl. Math. Model.*, **35**, 781-796.
Meziane, M.A.A., Abdelaziz, H.H. and Tounsi, A.T. (2014), "An efficient and simple refined theory for buckling and free vibration of exponentially graded sandwich plates under various boundary conditions", *J. Sandw. Struct. Mater.*, **16**(3), 293-318.
Mori, T. and Tanaka, K. (1973), "Average stress in matrix and average elastic energy of materials with misfitting inclusions", *Acta Metall. Mater.*, **21**, 571- 574.
Motezaker, M. and Kolahchi, R. (2017), "Seismic response of SiO2 nanoparticles-reinforced concrete pipes based on DQ and newmark methods", *Comput. Concrete*, **19**, 751-759.
Mouffoki, A., Adda Bedia, E.A., Houari, M.S.A. and Hassan, S. (2017), "Vibration analysis of nonlocal advanced nanobeams in hygro-thermal environment using a new two-unknown trigonometric shear deformation beam theory", *Smart Struct. Syst.*, **20**(3), 369-383.
Paidoussis, M.P. and Li, G.X. (1993), "Pipes conveying fluid: a model dynamical problem", *J. Fluid. Struct.*, **7**, 137-204.
Rafiee, R. and Moghadam, R.M. (2012), "Simulation of impact and post-impact behavior of carbon nanotube reinforced polymer using multi-scale finite element modelling", *Comput. Mater. Sci.*, **63**, 261-266.
Reddy, J.N. (1984), "A simple higher order theory for laminated composite plates", *J. Appl. Mech.*, **51**, 745-752.
Safari Bilouei, B., Kolahchi, R. and Rabani Bidgoli, M. (2016), "Buckling of concrete columns retrofitted with Nano-Fiber Reinforced Polymer (NFRP)", *Comput. Concrete*, **18**, 1053-1063.
Shen, H. and Xiang, Y. (2012), "Nonlinear vibration of nanotube-reinforced composite cylindrical shells in thermal environments", *Comput. Meth. Appl. Mech. Eng.*, **213**, 196-211.
Shi, D.L. and Feng, X.Q. (2004), "The effect of nanotube waviness and agglomeration on the elastic property of carbon nanotube-reinforced composties", *J. Eng. Mater. Tech ASME*, **126**, 250-270.
Thomas, B. and Roy, T. (2016), "Vibration analysis of functionally graded carbon nanotube-reinforced composite shell structures", *Acta Mech.*, **227**, 581-599.
Toorani, M.H. and Lakis, A.A. (2001), "Dynamic analysis of anisotropic cylindrical shells containing flowing fluid", *J. Press. Ves. Technol. Trans. ASME*, **123**, 454-60.
Vodenitcharova, T. and Zhang, L. (2006), "Bending and local buckling of a nanocomposite beam reinforced by a single-walled carbon nanotube", *Int. J. Solid. Struct.*, **43**(10), 3006-3024
Wang, L. and Ni, Q. (2009), "A reappraisal of the computational modelling of carbon nanotubes conveying viscous fluid", *Mech. Res. Commun.*, **36**, 833-837.
Yahia, S.A., Hassen, A.A., Houari, M.S.A. and Tounsi, A. (2015), "Wave propagation in functionally graded plates with porosities using various higher-order shear deformation plate theories", *Struct. Eng. Mech.*, **53**(6), 1143-1165.
Zemri, A., Houari, M.S.A., Bousahla, A.A. and Tounsi, A. (2015), "A mechanical response of functionally graded nanoscale beam: an assessment of a refined nonlocal shear deformation theory beam theory", *Struct. Eng. Mech.*, **54**(4), 693-710.
Zhang, T., Ouyang, H., Zhang, Y.O. and Lv, B.L. (2016), "Nonlinear dynamics of straight fluid-conveying pipes with general boundary conditions and additional springs and masses", *Appl. Math. Model.*, **40**(17-18), 7880-7900.
Zhang, Y.L., Reese, J.M. and Gorman, D.G. (2002), "Initially tensioned orthotropic cylindrical shells conveying fluid: A vibration analysis", *J. Fluid. Struct.*, **16**(1), 53-70.
Zidi, M., Tounsi, A. and Bég, O.A. (2014), "Bending analysis of FGM plates under hygro-thermo-mechanical loading using a four variable refined plate theory", *Aerosp. Sci. Tech.*, **34**, 24-34.

CC

Appendix

$$K = K_{out}\left[1+\frac{\xi\left(\frac{K_{in}}{K_{out}}-1\right)}{1+\alpha\left(1-\xi\right)\left(\frac{K_{in}}{K_{out}}-1\right)}\right], \quad (A1)$$

$$G = G_{out}\left[1+\frac{\xi\left(\frac{G_{in}}{G_{out}}-1\right)}{1+\beta\left(1-\xi\right)\left(\frac{G_{in}}{G_{out}}-1\right)}\right], \quad (A2)$$

where

$$K_{in} = K_m + \frac{\left(\delta_r - 3K_m\chi_r\right)C_r\zeta}{3\left(\xi - C_r\zeta + C_r\zeta\chi_r\right)}, \quad (A3)$$

$$K_{out} = K_m + \frac{C_r\left(\delta_r - 3K_m\chi_r\right)\left(1-\zeta\right)}{3\left[1-\xi-C_r\left(1-\zeta\right)+C_r\chi_r\left(1-\zeta\right)\right]}, \quad (A4)$$

$$G_{in} = G_m + \frac{\left(\eta_r - 3G_m\beta_r\right)C_r\zeta}{2\left(\xi - C_r\zeta + C_r\zeta\beta_r\right)}, \quad (A5)$$

$$G_{out} = G_m + \frac{C_r\left(\eta_r - 3G_m\beta_r\right)\left(1-\zeta\right)}{2\left[1-\xi-C_r\left(1-\zeta\right)+C_r\beta_r\left(1-\zeta\right)\right]}, \quad (A6)$$

where χ_r, β_r, δ_r, η_r may be calculated as

$$\chi_r = \frac{3\left(K_m+G_m\right)+k_r-l_r}{3\left(k_r+G_m\right)}, \quad (A7)$$

$$\beta_r = \frac{1}{5}\left\{\frac{4G_m+2k_r+l_r}{3\left(k_r+G_m\right)}+\frac{4G_m}{\left(p_r+G_m\right)}+\frac{2\left[G_m\left(3K_m+G_m\right)+G_m\left(3K_m+7G_m\right)\right]}{G_m\left(3K_m+G_m\right)+m_r\left(3K_m+7G_m\right)}\right\}, \quad (A8)$$

$$\delta_r = \frac{1}{3}\left[n_r+2l_r+\frac{\left(2k_r-l_r\right)\left(3K_m+2G_m-l_r\right)}{k_r+G_m}\right], \quad (A9)$$

$$\eta_r = \frac{1}{5}\left[\frac{2}{3}\left(n_r-l_r\right)+\frac{4G_m p_r}{\left(p_r+G_m\right)}+\frac{8G_m m_r\left(3K_m+4G_m\right)}{3K_m\left(m_r+G_m\right)+G_m\left(7m_r+G_m\right)}+\frac{2\left(k_r-l_r\right)\left(2G_m+l_r\right)}{3\left(k_r+G_m\right)}\right]. \quad (A10)$$

where, K_m and G_m are the bulk and shear moduli of the matrix which can be written as

$$K_m = \frac{E_m}{3\left(1-2\upsilon_m\right)}, \quad (A11)$$

$$G_m = \frac{E_m}{2\left(1+\upsilon_m\right)}. \quad (A12)$$

Furthermore, β, α can be obtained from

$$\alpha = \frac{\left(1+\upsilon_{out}\right)}{3\left(1-\upsilon_{out}\right)}, \quad (A13)$$

$$\beta = \frac{2\left(4-5\upsilon_{out}\right)}{15\left(1-\upsilon_{out}\right)}, \quad (A14)$$

$$\upsilon_{out} = \frac{3K_{out}-2G_{out}}{6K_{out}+2G_{out}}. \quad (A15)$$

where two parameters ξ and ζ describe the agglomeration of nanoparticles as

$$\xi = \frac{V_{inclusion}}{V}, \quad (A16)$$

$$\zeta = \frac{V_r^{inclusion}}{V_r}. \quad (A17)$$

However, the average volume fraction c_r of nanoparticles in the composite is

$$C_r = \frac{V_r}{V}. \quad (A18)$$